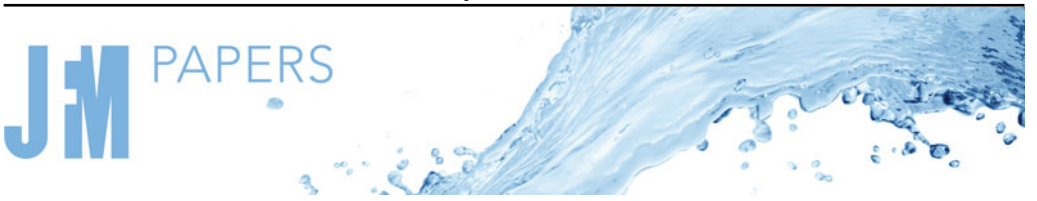
J. Fluid Mech. (2025), *vol.* 1023, A17, doi:10.1017/jfm.2025.10837



Fluidic levitation of bubbles, drops and solid spheres

James S. Sharp[1] **and Anna Kalogirou**[2]

[1]School of Physics and Astronomy, University of Nottingham, University Park, Nottingham NG7 2RD, UK

[2]School of Mathematical Sciences, University of Nottingham, University Park, Nottingham NG7 2RD, UK

Corresponding author: James S. Sharp, james.sharp@nottingham.ac.uk

(Received 21 July 2025; revised 15 September 2025; accepted 13 October 2025)

Fluidic levitation of different types of objects is achieved using laboratory experiments and described using simple mathematical models. Air bubbles, liquid tetrabromoethane droplets and solid spherical polytetrafluoroethylene beads were levitated in flowing water inside vertically oriented cylindrical tubes having diameters of 5, 8 and 10 mm. The centre of mass of all levitated objects was observed to undergo horizontal oscillations once a stable levitation point had been established. A simple model that considers the balance of gravitational, buoyancy and drag forces (as well as wall effects) was used to successfully predict the flow rates that are required to obtain stable levitation of objects with a range of different sizes. Horizontal motion was shown to be driven by vortex shedding of the objects in the tubes, and the dependence of the frequency of oscillation on their size was predicted.

Key words: drops and bubbles, vortex shedding

1. Introduction

Levitation is the process of suspending individual objects such as particles, droplets or bubbles within a contact-free environment. This is particularly useful for simulating microgravity conditions, studying particle collision dynamics, bubble/droplet coalescence and measuring forces and pressures. Researchers have explored multiple methods for levitation of objects, including acoustic, magnetic, optical, aerodynamic and electrostatic/electrodynamic levitation (Ashkin 1986; Geim & Berry 1997; Hyers & Rogers 2008; Mirica *et al.* 2009; Friend & Yeo 2011; Foresti *et al.* 2013; Lu, Zhang & Li 2013).

© The Author(s), 2025. Published by Cambridge University Press. This is an Open Access article, distributed under the terms of the Creative Commons Attribution licence (https://creativecommons.org/licenses/by/4.0/), which permits unrestricted re-use, distribution and reproduction, provided the original article is properly cited.

https://doi.org/10.1017/jfm.2025.10837 Published online by Cambridge University Press

An alternative approach is to use fluidic levitation – a process of suspending objects using fluid flow. Fluidic levitation is relevant in numerous applications including microscale control in microfluidic devices (Ding *et al.* 2013), non-contact manipulation of fragile or reactive materials such as biological samples (Marzo *et al.* 2015) and production of clean environments in electronics or pharmaceutical manufacturing where contamination must be minimised (Trinh 1985). Typical configurations include flow in narrow channels or pipes, and Stokes flow-based apparatus for micron-scale particles (Kirby 2010). A popular example of fluidic levitation involves the suspension of a ball in a fluid (air or water) jet due to combined Bernoulli and Coanda effects (Mejia-Alvarez, Ohtake & Foss 2021). Lubrication induced levitation of spheres has also been recently observed by Ockendon, Ockendon & Mullin (2024).

Fluidic levitation relies upon control of fluid flow in order to generate a drag force that balances gravitational and buoyancy forces. At the levitation point, a force balance is achieved and the object remains suspended with its terminal speed equal and opposite to that of the suspending fluid (Mendelson 1967). The motion of a small object within a fluid depends on a complex interplay of forces (buoyancy, drag, inertia, lift forces) and the Reynolds number associated with the flow (Clift, Grace & Webster 1978; Happel & Brenner 1983). In the absence of flow, the object will experience sedimentation or rising depending on the density difference with the surrounding fluid. When a background shear flow (e.g. Poiseuille) is applied, the behaviour of the object depends upon the flow rate.

At low Reynolds numbers ($Re \ll 1$), particles move steadily in the fluid, often migrating across streamlines due to shear-induced lift forces (Cappello *et al.* 2023). Bubbles and droplets in creeping flow have a tendency to maintain their shape because of surface tension forces, especially if their size is small. In confined flows, e.g. in pipes or channels, wall effects alter the velocity field around objects (Brenner 1962) and lubrication forces can generate lateral flows (Feng, Huz & Joseph 1994; Takemura *et al.* 2002; Magnaudet, Takagi & Legendre 2003; Stan *et al.* 2013; Manica *et al.* 2016*a*). At intermediate Reynolds numbers ($1 < Re \lessapprox 1000$), inertial effects become important and levitated objects may be seen to oscillate, spiral or follow a zigzag motion (Mathai *et al.* 2017). Such oscillatory motion is caused by vortex shedding (Lunde & Perkins 1998; She *et al.* 2021; Liu *et al.* 2023), leading to an unstable wake behind the particle which in turn generates oscillating lift forces (Oguz & Prosperetti 1998). In such flow regimes, bubbles and droplets may experience shape deformations (Chan & Leal 1979) resulting in the formation of oblate spheroids (Herrada & Eggers 2023). Coupling of flow-induced deformations in the bubble shape with shedding of vortices can generate a horizontal component to the bubble velocity (Liu *et al.* 2023). At high Reynolds numbers ($Re \gg 1000$), the flow becomes turbulent and the object follows a chaotic trajectory with complex vortex shedding dynamics (Horowitz & Williamson 2010).

In this paper, we combine experiments with a simple model of fluidic levitation that considers the effects of gravity, buoyancy and drag forces (including wall effects). This is applied to the study of air bubbles, liquid droplets and solid spherical beads/particles. A simple force balance is shown to be able to predict the flow rates required for the levitation of objects of different sizes in vertically oriented tubes having different internal diameters. All of the objects studied are observed to undergo centre-of-mass oscillations perpendicular to the axis of the tubes. This is interpreted in the context of vortex shedding and a simple mathematical model is shown to give good agreement with the measured size dependence of the vibrational frequencies of the objects.

https://doi.org/10.1017/jfm.2025.10837 Published online by Cambridge University Press

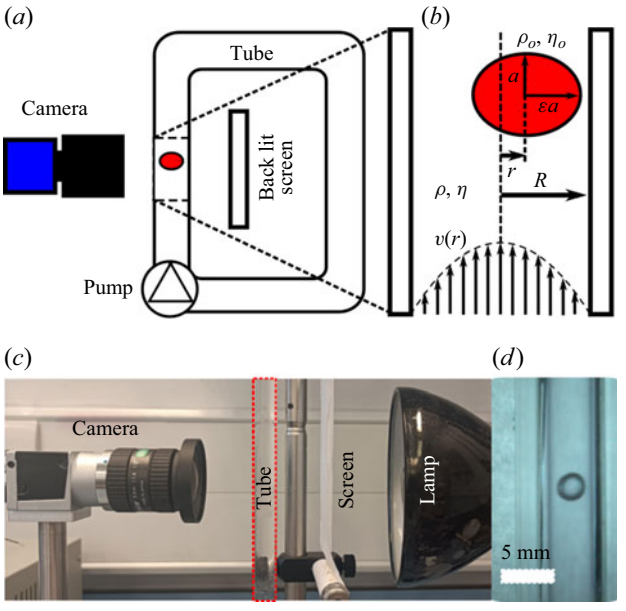


Figure 1. Panel (*a*) shows a schematic diagram of the experimental set-up, where a 12 V DC pump is used to force water through a closed loop and thereby levitate solid particles, liquid droplets or air bubbles. Panel (*b*) shows a schematic section of the tube where the objects are levitated and defines the parameters used in the model (see text for definitions of all parameters). Panels (*c*) and (*d*) show images of the experimental set-up and a levitated air bubble inside a 5 mm diameter tube, respectively.

2. Experimental

Air bubbles were levitated inside cylindrical glass tubes of length 300 mm having different internal diameters whose axes were oriented vertically (figure 1*a*,*b*). Flexible PVC tubing having the same internal diameter as the glass tubing was used to connect it to a 12 V variable speed DC water pump and to create a closed circulating loop. A syringe was used to inject individual bubbles of different sizes. These bubbles were observed to rise inside the tube under the action of buoyancy until they reached terminal speed. Water was pumped down the tube to slow the rise of the bubbles and they were imaged using a Basler ace ACa800-510uc camera with a Computar H0514-MP, 5 mm focal length lens attached to it. The tube was back lit by placing an LED lamp behind a white paper screen (figure 1*c*) to enable the bubbles to be thresholded against the background. The resolution of the optical system corresponded to 0.06 mm per pixel.

Software written in Python was used to track the position of the bubbles and to vary the voltage applied to the DC pump. This was done to obtain a stable downward flow rate where the local speed of the water matched the terminal speed of the rising bubbles and caused them to levitate in the tube (figure 1*d*). This created a neutral equilibrium and the position of the levitated bubbles could be controlled and maintained at any point in the straight section of the vertical section of the tube. In each case, the dimensions of the bubbles and the flow rates required to levitate them were recorded. This was repeated for glass tubes with internal diameters of 5, 8 and 10 mm and for bubbles with a range of sizes (bubble widths) between 0.4 and 10 mm – the upper limit of the bubble width being set by the internal diameter of the tube. Bubbles in the 5 mm diameter tube were observed to retain a near-spherical shape during the levitation experiments. For larger tube sizes, the

https://doi.org/10.1017/jfm.2025.10837 Published online by Cambridge University Press

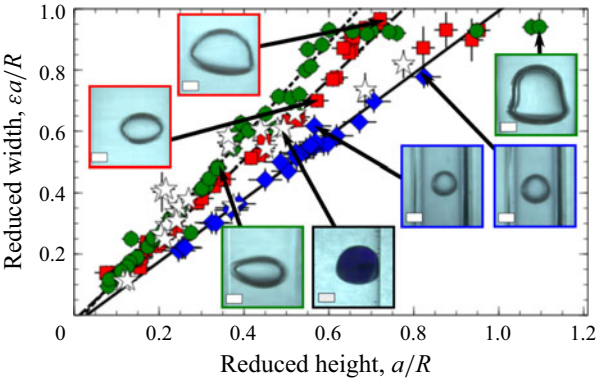


Figure 2. Aspect ratio of air bubbles and tetrabromoethane droplets. Data shown are for the reduced half-width ($\epsilon a/R$) plotted as a function of the reduced height (a/R). The white stars correspond to tetrabromoethane droplets levitated inside a 10 mm diameter tube, while the remaining symbols correspond to air bubbles levitated inside tubes with internal diameters of 5 mm (blue diamonds), 8 mm (red squares) and 10 mm (green circles), respectively. The lines are fits and provide the values of the aspect ratio ϵ for each data set. The slopes give $\epsilon = 1.02 \pm 0.05$ (solid), $\epsilon = 1.31 \pm 0.04$ (dashed) and $\epsilon = 1.54 \pm 0.05$ (dotted), respectively. The images shown as insets present bubble and droplet shapes at different aspect ratios. Scale bars correspond to 2 mm in each image.

bubbles were observed to distort into the shape of oblate spheroids (see figure 2). Large bubbles (with widths comparable to the tube diameter) became elongated and bell shaped.

Similar experiments were repeated using liquid droplets of tetrabromoethane (Sigma Aldrich, Gillingham, UK) and solid, spherical polytetrafluoroethylene (PTFE) beads. Tetrabromoethane was chosen for the liquid droplets because of its high density and poor miscibility with water. The fact that the density of tetrabromoethane is similar to that of PTFE enabled us to compare the results obtained for the deformable liquid droplets directly with those for the solid spheres. In these experiments, the tetrabromoethane droplets were stained with Oil Red dye (Sigma Aldrich, Gillingham, UK) to provide optical contrast between the droplet and water. This enabled the droplets to be imaged more easily. Both the solid beads and liquid droplets were levitated inside a glass tube with an internal diameter of 10 mm. In these experiments, water was pumped upward through the tube because both tetrabromoethane and PTFE have densities that are significantly higher than that of water (see table 1). The tetrabromoethane droplets were observed to form oblate spheroids (see figure 2) in the flow while the PTFE beads remained spherical. The reason for using only the larger tube for the liquid drops was largely related to experimental difficulties associated with injecting the drops into smaller diameter tubes. For the smaller tubes the tetrabromoethane drops would often stick to the walls of the tube and contaminate the flow. While a similar effect was observed for the bubbles sticking to the tube walls in smaller tubes, they were relatively easy to remove by temporarily increasing the flow rate in the tube. On the other hand, the solid sphere levitation experiments were restricted due to the availability of a suitable range of sphere diameters. These spheres were only available in diameter increments of $\sim$1 mm, and hence using only the larger tube diameter would ensure that sufficient data would be collected.

Small objects (bubbles, droplets and beads) having widths less than $\sim$0.3 of the tube diameter had a tendency to levitate off centre at a position approximately 3/5 of the radius of the tube, as observed previously by Segre & Silberberg (1962). Larger objects tended to be located more centrally. Segre & Silberberg (1962) attributed the off-centre position of small objects to the inertia of the flowing fluid in the tube, mentioning the

https://doi.org/10.1017/jfm.2025.10837 Published online by Cambridge University Press

Material	Physical state	Density (kg m^{-3})	Viscosity (Pa s)
Water	Liquid	997	0.89×10^{-3}
Air	Gas	1.29	1.81×10^{-5}
Tetrabromoethane	Liquid	2970	10.94×10^{-3}
Polytetrafluoroethylene (PTFE)	Solid	2200	∞

Table 1. Physical properties of materials at room temperature.

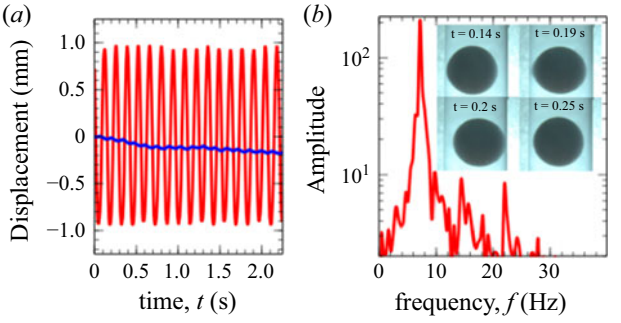


Figure 3. Motion of a levitated PTFE bead. Panel (*a*) shows the horizontal (red line) and vertical (blue line) displacement of an 8 mm diameter PTFE bead levitating in flow inside a 10 mm diameter tube. Panel (*b*) shows the power spectrum of the horizontal motion data, obtained by Fourier transformation of the data in the left panel. The inset in panel (*b*) shows examples of images of the position of the bead taken at different times during its motion.

potential importance of rotation and the generation of Magnus forces in the context of solid particles.

All of the levitating objects were observed to undergo horizontal oscillations once a stable levitation flow rate had been achieved. The frequency of these oscillations was found to depend upon the size/width of the object being levitated and the internal diameter of the tube. Short movies (typically 2 s long) of the motion of each type of levitated object were captured at 200 frames per second using the same camera that was used to track the object positions. Software was written in Python to analyse these short movies, extract the size (height and width) of the objects and to track the oscillatory motion. Figure 3 shows an example of the variation in horizontal (red line) and vertical (blue line) positions of a 8 mm diameter PTFE bead levitating inside a 10 mm diameter tube. The second panel in figure 3 shows a plot of the power spectrum of the horizontal motion data which contains a distinct peak corresponding to the frequency of the oscillations. In all of the experiments performed here, the oscillatory motion of the objects was found to be highly periodic – no evidence of aperiodic or chaotic motion was observed.

3. Results and discussion

3.1. *Levitation condition*

Different types of objects, including solid spherical beads, oblate spheroidal liquid droplets and bubbles, were suspended by a moving flow inside a cylindrical tube of inner radius R, whose axis is oriented vertically (see figure 1*b*,*d*). All spherical objects are taken to have radius a, while oblate spheroidal objects are assumed to have smallest diameter (usually the height) equal to $2a$ and largest diameter (usually the width) equal to $2\epsilon a$.

https://doi.org/10.1017/jfm.2025.10837 Published online by Cambridge University Press

In what follows, we will derive the levitation condition for general objects of aspect ratio $\epsilon \geqslant 1$, and will set $\epsilon = 1$ when dealing specifically with spherical objects.

The sum of gravity and buoyancy forces felt by the object is given by

$$F_g = \frac{4}{3}\pi\epsilon^2 a^3 \Delta\rho g, \tag{3.1}$$

where g is the acceleration due to gravity and $\Delta\rho$ is the density difference between the object material, ρ_o, and the suspending fluid, ρ. The object also experiences a drag force inside the moving fluid which opposes its motion. This force is dependent upon the shape and type of object and can be written as

$$F_d = 6\pi\eta\epsilon a\gamma\lambda v(r), \tag{3.2}$$

where η is the viscosity of the suspending fluid, $v(r)$ is the speed of the fluid at a distance r from the tube centre (see figure 1*b*), γ is a blocking factor and $\lambda = \lambda(a, R)$ is a form factor that accounts for the effects of the drag on the object caused by its shape and proximity to the walls.

The blocking factor γ arises because the presence of the object in the tube blocks the flow. The restriction in flow caused by the blockage leads to a pressure build-up across the object in the axial direction of the tube. This build-up of pressure has the effect of increasing the drag on the object in a tube relative to that in an unbounded flow and gives rise to a doubling in the effective drag force (Clift *et al.* 1978). We will hence set $\gamma = 2$ in the drag force (3.2).

Values of the parameter λ have been calculated for solid spherical particles and slightly distorted fluid spheres in a moving fluid inside a cylinder (Stokes' approximation for the hydrodynamic equations for slow flow; Haberman & Sayre 1958). This approach leads to power-law expansions for the parameter λ for the levitated objects of the form

$$\lambda = \frac{2\left(1+\frac{2}{3}\sigma\right) - \frac{2}{3}\xi^2 - 0.96074(1-\sigma)\xi^5}{(1+\sigma) - 2.105\left(1+\frac{2}{3}\sigma\right)\xi + 2.0865\,\xi^3 - 1.7068\left(1-\frac{2}{3}\sigma\right)\xi^5 + 0.726(1-\sigma)\xi^6}, \tag{3.3}$$

where $\xi = a/R$ and $\sigma = \eta/\eta_o$ is the viscosity ratio between the suspending fluid and the levitated object. In the case of solid particles, we set η_o to be infinite and $\sigma = 0$. Values of σ for bubbles and liquid droplets were determined using the data in table 1. Figure 4 shows the variation in λ for solid spheres, liquid droplets and air bubbles in tubes of different internal diameters. As expected, the functional form of the drag force on the particle (cf. (3.2) and (3.3)) is consistent with motion in an unbounded flow when the objects are small, and increases monotonically as the object size approaches the tube diameter and hence wall effects become more significant.

Far from the object, the speed of the suspending fluid is assumed to be determined by Poiseuille flow, i.e.

$$v(r) = v_m\left(1 - \left(\frac{r}{R}\right)^2\right), \qquad \text{and} \qquad Q = \int_0^{2\pi}\int_0^R v(r)\, r\, \mathrm{d}r\mathrm{d}\theta = \frac{\pi R^2}{2} v_m, \tag{3.4a,b}$$

where v_m is the maximum speed achieved at the centre of the tube, and Q is the volumetric flow rate. We note that, while the background flow speed is valid for $0 \leqslant r \leqslant R$, the object's centre of mass only experiences fluid speeds for $0 \leqslant r \leqslant R - \epsilon a$. If the object's terminal speed in the tube matches the speed of the suspending fluid, then the two forces in (3.1) and (3.2) balance and the object will appear to levitate in the frame of reference of an external observer. Setting $F_g = F_d$ and combining with (3.4*a*,*b*), provides an expression

https://doi.org/10.1017/jfm.2025.10837 Published online by Cambridge University Press

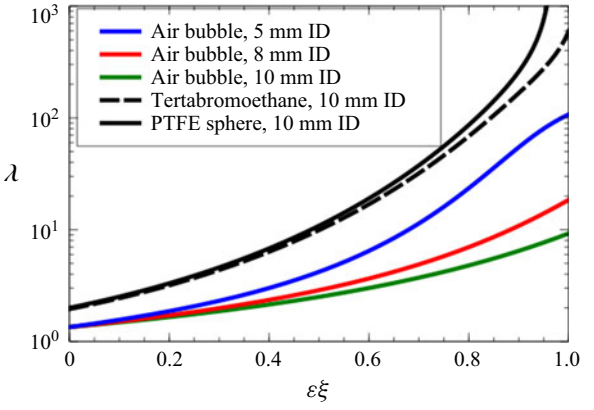


Figure 4. Variation of parameter λ as a function of the reduced half-width ($\epsilon\xi = \epsilon a/R$) of the levitating object, obtained from (3.3) for air bubbles in 5 mm (blue line), 8 mm (red line) and 10 mm (green line) inner diameter tubes. Curves are also plotted for solid PTFE spheres (black solid line) and liquid tetrabromoethane droplets (black dashed line) in 10 mm diameter tubes. For each curve, the value of the viscosity ratio σ was determined from table 1. The values of the aspect ratio ϵ used for bubbles and droplets were obtained from the fits to the data in figure 2, while $\epsilon = 1$ was used for the solid spheres.

for the flow rate that is required to levitate the object, given by

$$Q_{lev} = \frac{\pi \epsilon a^2 R^2 \Delta\rho g}{9\eta\lambda\gamma \left(1 - \left(\frac{r}{R}\right)^2\right)}. \tag{3.5}$$

Figure 5 shows a comparison between the measured and calculated levitation flow rates for objects of different sizes. Results are presented for solid PTFE beads, liquid tetrabromoethane droplets and air bubbles. In all cases where the objects levitated off centre in the tube, the experimentally determined levitation flow rates were corrected by a factor of $1 - (r/R)^2$, with r set to the experimentally observed off-centre position. Correcting experimental flow rate data in this way enabled a simplified form of (3.5) to be used by setting $r = 0$ for all solid lines presented in figure 5. The values of λ used to generate the theoretical lines are calculated using (3.3), with viscosity ratios taken from the parameters of table 1. Density values were also taken from table 1 and values of ϵ were obtained from the fits to the data in figure 2.

The experimentally determined values of ϵ that were obtained for the bubbles and drops can be compared directly with the predictions of a simple model proposed by Manica *et al.* (2016*b*). These authors derived an expression for ϵ by balancing the inertial pressure due to the flow and the internal Laplace pressure of a bubble. We apply their approach to write the aspect ratio of the bubbles using the notation developed here, to obtain

$$\epsilon = \left(1 - \frac{9a\rho Q_{lev}^2}{16\pi^2 R^4 \gamma_{lo}}\right)^{-1}, \tag{3.6}$$

where γ_{lo} is the interfacial tension between the suspending liquid and the deformable object (bubble or drop). If we consider bubbles with $a = 0.4R$ (corresponding to the rough position of the maximum in the flow rate curves) and use the results of figure 5, we obtain levitation flow rates of approximately 1.5, 7 and 12 ml s^{-1} for bubbles in 5, 8 and 10 mm diameter tubes, respectively. Assuming a value of $\gamma_{lo} = 72 \times 10^{-3}$ J m^{-2} (surface tension of water/air interfaces at room temperature), the corresponding values

https://doi.org/10.1017/jfm.2025.10837 Published online by Cambridge University Press

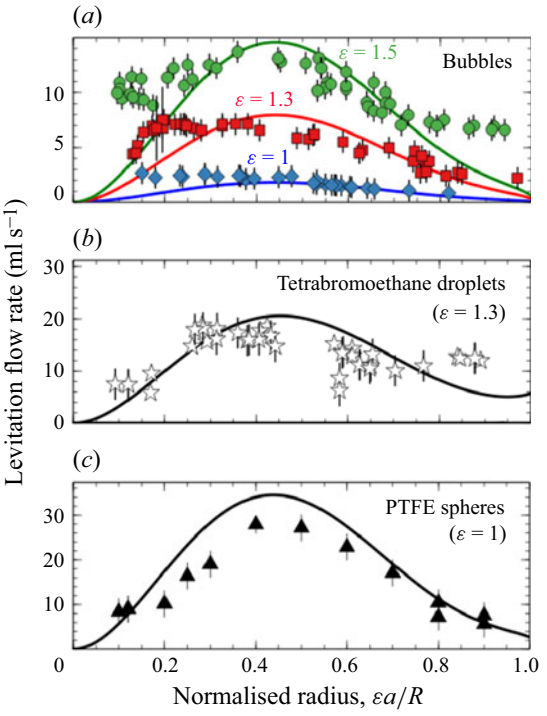


Figure 5. Flow rate for levitation of (*a*) air bubbles, (*b*) liquid tetrabromoethane droplets and (*c*) solid PTFE particles as a function of the normalised half-width, $\epsilon a/R$, of the object being levitated. Panel (*a*) shows data for air bubbles levitated inside tubes with internal diameters of 5 mm (blue diamonds), 8 mm (red squares) and 10 mm (green circles). Equation (3.5) was used to generate the solid lines using material parameters given in table 1.

of ϵ that we calculate using (3.6) are 1.05, 1.32 and 1.57. These values are broadly in agreement with the experimental values obtained for air bubbles from figure 2. Application of the same approach to the tetrabromoethane droplets yields a value of $\epsilon = 1.34$ using $\gamma_{lo} = 72 \times 10^{-3}$ J m^{-2} or $\epsilon = 1.57$ using $\gamma_{lo} = 50 \times 10^{-3}$ J m^{-2} (a typical value for alkane/water and haloalkane/water interfaces; Israelachvili 1991). Some disagreement between the values of ϵ predicted by (3.6) and the data for tetrabromoethane is to be expected when using appropriate values for γ_{lo}. This equation was developed by Manica *et al.* (2016*b*) for a compressible gas bubble and as such neglects the influence of viscosity and incompressibility that are expected to be important in a liquid droplet.

The results of figure 5 indicate that the shapes of the experimental data are broadly in agreement with those of the model predicted by (3.5). While the level of agreement shown is generally good, the model proposed here clearly fails to describe the behaviour of the levitating system for certain values of the normalised half-width of the levitated object. This is true for small ($\epsilon a/R < 0.3$) bubbles, and both large ($\epsilon a/R > 0.7$) bubbles and liquid droplets, where the experimentally determined flow rates are higher than those predicted by the model. In the case of the spheres, the shape of the flow rate curve predicted by (3.5) is similar that observed in experiments. However, a simple scaling of the solid line in the bottom panel of figure 5 by a factor of $\sim$1.1 is required to obtain good agreement between the model and the experimental data. This factor could be accounted for in terms of uncertainties in the parameters in table 1.

Disagreement between the data and the simple model is not entirely unexpected. For example, the model neglects the effects of compressibility and the time-dependent shape

https://doi.org/10.1017/jfm.2025.10837 Published online by Cambridge University Press

deformations of bubbles and droplets in the flow, which will significantly influence the values of λ used for larger objects. The assumption that the far-field speed profile obtained for Poiseuille flow in a tube is valid close to the levitating objects is also a crude one. This is potentially further complicated by the use of a relatively short length of the straight section of the glass tube used to levitate the objects. The use of a short circulation loop is likely to make it more difficult to establish laminar flow in the presence of a levitating object. Ideally a longer vertical section of the tube would have been used to perform these experiments and allow the Poiseuille flow profile to be better established. However, disturbances caused by fluctuations in the flow due to the pump were found to have a significant effect on the stability of the levitation condition. A low noise pump with a low flow rate was therefore chosen to minimise background disturbances in the flow. The choice of pump limited the pressure range available and therefore the height of the fluid column that could be used to obtain a wide enough range of levitation flow rates in the experiments.

In addition to the above factors, the range of validity of the Reynolds numbers associated with (3.3) are a potential source of disagreement. We estimate the Reynolds numbers attained in these experiments to be $Re \sim 600$, while (3.3) was developed for systems where $Re = \mathcal{O}(1)$ (Clift *et al.* 1978).

3.2. *Oscillatory motion of objects*

The oscillatory motion of bubbles, drops and solid beads can be explained by the process of vortex shedding. This mechanism has been shown to be responsible for the zigzag and helical motion of bubbles rising in quiescent liquids (Lunde & Perkins 1998; Liu *et al.* 2023) and small diameter tubes (Ortiz-Villafuerte, Schmidl & Hassan 2001). High-speed movies of solid particles levitated in the tubes studied here confirm that vortex shedding also occurs when mica powder particles are added to the water (see Supplementary Information Movie 1.mp4).

In what follows, a simple model is derived using a similar approach to that described by Baker (2016). We begin with the definition of the Strouhal number, St, a dimensionless parameter that describes oscillating flow mechanisms. It can be used to set the frequency of vortex shedding, f, behind an object of width w in a flow of speed v_o, and it is defined by

$$St = \frac{f w}{v_o}. \tag{3.7}$$

The Strouhal number has been reported in the literature to be approximately equal to 0.2 for most Reynolds numbers (Baker 2016). In the case of an incompressible fluid, the same flow rate should be maintained everywhere and hence the product of fluid speed and cross-sectional area should be constant, both when considered around the edges of the object or far away.

When an object of cross-sectional area A moves in a tube of radius R, this condition becomes

$$v_o(\pi R^2 - A) = v_m \pi R^2 \qquad \Leftrightarrow \qquad v_o = \frac{v_m \pi R^2}{(\pi R^2 - A)}, \tag{3.8a,b}$$

where we have assumed that the characteristic fluid speed far away from the object is set by v_m from (3.4*a*). Inserting (3.8*b*) into (3.7) and using (3.4*b*) to eliminate the maximum fluid speed, we obtain an equation for the vortex shedding frequency of an oblate spheroid

https://doi.org/10.1017/jfm.2025.10837 Published online by Cambridge University Press

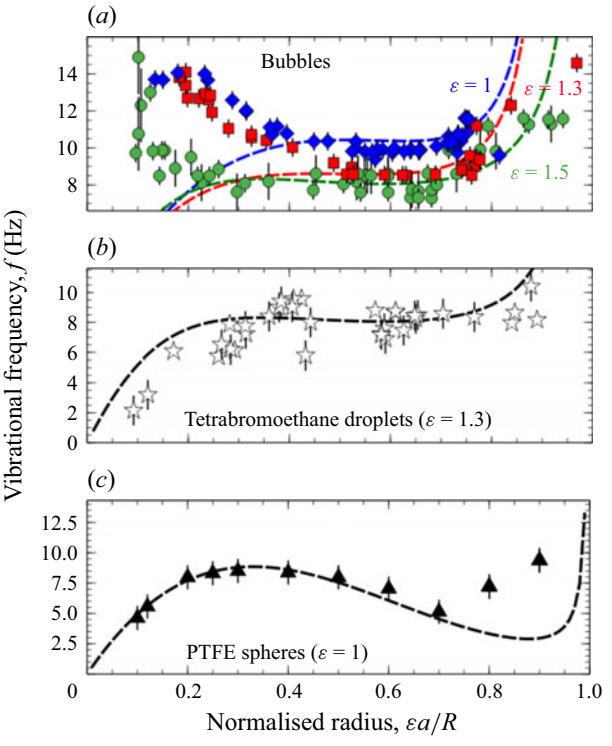


Figure 6. Vibrational frequencies of (*a*) air bubbles, (*b*) liquid tetrabromoethane droplets and (*c*) solid PTFE particles as a function of the normalised half-width, $\epsilon a/R$, of the levitated objects. Panel (*a*) shows data for air bubbles levitated inside tubes with internal diameters of 5 mm (blue diamonds), 8 mm (red squares) and 10 mm (green circles). Equation (3.9) was used to generate the dashed lines using material parameters given in table 1.

of the form

$$f = \frac{Q_{lev}}{5\pi\epsilon a\left(R^2 - \epsilon^2 a^2\right)}, \tag{3.9}$$

where we have set $w = 2\epsilon a$ and $A = \pi\epsilon^2 a^2$ for the width and cross-sectional area, respectively. Here, we have assumed that the frequency of vibration is set by the speed of the fluid around the edges of the object as this is where vortex shedding occurs. This is different to the speed used to determine the levitation condition, where form drag ((3.2) and (3.3)) is important and the speed of fluid incident on the surface of the object presented to the flow is more appropriate.

Figure 6 shows a comparison between the results of (3.9) and the measured vibrational frequencies of air bubbles, tetrabromoethane drops and solid PTFE particles as a function of the size of the levitating object in tubes of different radii. The values of the levitation flow rate obtained using (3.5) (see also figure 5) were inserted into (3.9) and used to generate the dashed lines in figure 6. The frequencies predicted by the simple model are clearly comparable to the measured vibrational frequencies, and the functional form predicted using vortex shedding arguments captures the essential physics of the oscillatory motion.

If we assume that the behaviour of small objects can be taken as indicative of the behaviour of an object in an unbounded flow, we see from figure 6 that the experimentally determined vibrational frequency (a proxy for the rate of vortex shedding) for bubbles is

https://doi.org/10.1017/jfm.2025.10837 Published online by Cambridge University Press

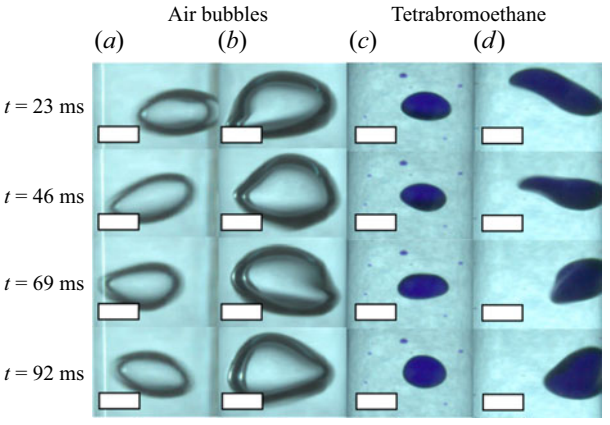


Figure 7. Examples of shape oscillations in air bubbles and liquid tetrabromoethane droplets inside 10 mm diameter tubes. Data in the first two columns correspond to air bubbles with values of $\epsilon a/R = 0.64$ (column a) or $\epsilon a/R = 0.80$ (column b), while data in the last two columns are for tetrabromoethane droplets with $\epsilon a/R = 0.42$ (column c) or $\epsilon a/R = 0.69$ (column d). The rows correspond to images captured at 23 ms time intervals. The scale bar in each image corresponds to 3 mm.

suppressed for intermediate object widths, but then increases as the width of the bubbles approaches the diameter of the tube. In the case of the liquid drops and solid particles, the agreement between data and model is improved. While there is a tendency for the vortex shedding rate (vibrational frequency) to plateau (with a small dip for the spheres around $\epsilon a/R \sim 0.7$), we again see an enhancement in the rate of vortex shedding when the flow around the objects becomes constricted.

Disagreement is observed between theory and experiments for the vibrational frequencies of small bubbles and large spheres. This is likely caused by similar failings of the model that was used to predict the flow rates shown in figure 5. Given that (3.9) predicts $f \propto Q_{lev}$, any failure to reproduce the experimentally determined levitation flow rates with the simple model will propagate and generate disagreement between the predicted and measured vibrational frequencies. An additional limitation of the vortex shedding model is that it neglects the parabolic flow profile inside the tube, using only the maximum speed, v_m, as the characteristic speed. This is likely to introduce some disagreement between the model and data in figure 6 for small objects that are offset from the centre of the tube and for large deformable objects such as bubbles, where the fluid speed changes considerably across their front surfaces.

The issue of shape oscillations in large deformable objects such as air bubbles and tetrabromoethane droplets is a particularly important consideration. Figure 7 shows examples of some of the shape changes observed in 10 mm diameter tubes. These images clearly show that the shapes of smaller bubbles and liquid droplets maintain a shape that is close to that of an oblate spheroid during the oscillatory motion (columns a and c). However, larger objects with $\epsilon a/R \sim 0.7$ and greater undergo large oscillations in shape and exhibit large deviations from a spheroidal shape (columns b and d). In cases such as these, we note that the values of $\epsilon a/R$ quoted represent time averages. Interestingly, these large deviations from the spheroidal shape correspond to regions in figures 5 and 6 where the experimental levitation flow rates and vibrational frequencies show deviations from the predictions of the simple model. A more detailed analysis of shape changes for large droplets and bubbles could provide better agreement between the model and the experimental data. This will be the subject of future work.

https://doi.org/10.1017/jfm.2025.10837 Published online by Cambridge University Press

In future we also hope to expand the work presented here to include levitation of non-spheroidal objects e.g. cylinders and other shapes with different aspect ratios. In particular, we will study their vortex shedding and vibrational properties. We will also develop experiments to levitate and manipulate multiple objects by application of pulsed flows and using shaped tubes.

4. Conclusions

Fluidic levitation is a versatile technique that enables contactless manipulation of solid particles, gas bubbles and liquid droplets by balancing fluid dynamic forces experienced by the object. In this work, fluidic levitation of objects of different sizes was achieved by flowing water in a tube. At a critical flow rate, forces due to gravity, buoyancy and drag on the objects were balanced, and the levitation condition was obtained by matching the flow speed with the object's terminal speed. Once a stable levitation point had been established, horizontal vibrational motion was observed for all the levitated objects. This motion was interpreted in terms of vortex shedding and a simple calculation using the definition of the Strouhal number was used to relate the frequency of oscillation of the objects to their size and the flow rate. Understanding the motion of small levitated objects in tubes, including the zigzag motion and wall effects, is critical for optimising fluidic levitation systems for applications ranging from biomedical devices to material processing.

Supplementary movie. Supplementary movie is available at https://10.1017/jfm.2025.10837.

Declaration of interests. The authors report no conflict of interest.

Data availability statement. The data that support the findings of this study are openly available in the Nottingham Research Data Management Repository at https://doi.org/10.17639/nott.7581.

References

Ashkin, A. 1986 Observation of a single-beam gradient force optical trap for dielectric particles. *Opt. Lett.* **11** (5), 288–290.

Baker, R.C. 2016 In *Flow Measurement Handbook*, 2nd edn, pp. 358–361. Cambridge University Press.

Brenner, H. 1962 Effect of finite boundaries on the Stokes resistance of an arbitrary particle. *J. Fluid Mech.* **12**, 35–48.

Cappello, J., Rivero-Rodriguez, J., Vitry, Y., Dewandre, A., Sobac, B. & Scheid, B. 2023 Beads, bubbles and drops in microchannels: stability of centred position and equilibrium velocity. *J. Fluid Mech.* **956**, A21.

Chan, P.C.-H. & Leal, L.G. 1979 The motion of a deformable drop in a second-order fluid. *J. Fluid Mech.* **92**, 131–170.

Clift, R., Grace, J.R. & Webster, M.E. 1978 *Bubbles, Drops and Particles*, pp. 221–243. Dover.

Ding, X. *et al.* 2013 Surface acoustic wave microfluidics. *Lab on a Chip* **13** (18), 3626–3649.

Feng, J., Huz, H.H. & Joseph, D.D. 1994 Direct simulation of initial value problems for the motion of solid bodies in a Newtonian fluid. Part 2. Couette and Poiseuille flows. *J. Fluid Mech.* **277**, 271–301.

Foresti, D., Nabavi, M., Klingauf, M., Ferrari, A. & Poulikakos, D. 2013 Acoustophoretic contactless transport and handling of matter in air. *Proc. Natl Acad. Sci.* **110** (31), 12549–12554.

Friend, J. & Yeo, L.Y. 2011 Microscale acoustofluidics: microfluidics driven via acoustics and ultrasonics. *Rev. Mod. Phys.* **83** (2), 647–704.

Geim, A.K. & Berry, M.V. 1997 Of flying frogs and levitrons. *Eur. J. Phys.* **18** (4), 307.

Haberman, W.L. & Sayre, R.M. 1958 Motion of rigid and fluid spheres in stationary and moving liquids inside cylindrical tubes. *Tech. Rep.* 1143. Dept. of Navy: David Taylor Model Basin.

Happel, J. & Brenner, H. 1983 *Low Reynolds Number Hydrodynamics*. Springer.

Herrada, M.A. & Eggers, J.G. 2023 Path instability of an air bubble rising in water. *Proc. Natl Acad. Sci.* **120**, e2216830120.

Horowitz, M. & Williamson, C.H.K. 2010 The effect of Reynolds number on the dynamics and wake structures of a freely rising and falling cylinder. *J. Fluid Mech.* **651**, 251–294.

https://doi.org/10.1017/jfm.2025.10837 Published online by Cambridge University Press

HYERS, R.W. & ROGERS, J.R. 2008 A review of electrostatic levitation for materials research. *High Temp. Mater. Process.* **27** (6), 461–474.

ISRAELACHVILI, J.N. 1991 *Intermolecular and Surfaces Forces*, 2nd edn, pp. 315. Academic Press.

KIRBY, B.J. 2010 *Micro- and Nanoscale Fluid Mechanics: Transport in Microfluidic Devices*. Cambridge University Press.

LIU, H., ZHANG, Y., WEI, Y., MU, Z., YANG, Y. & FAROOQ, M.S. 2023 Characteristics and mechanisms of the zigzag and spiral movement of rising bubbles in still water. *Appl. Sci.* **13**, 6500.

LU, W., ZHANG, S. & LI, J. 2013 Segregation driven by collision and coagulation of minor droplets in Al–Bi immiscible alloys under aerodynamic levitation condition. *Mater. Lett.* **107**, 340–343.

LUNDE, K. & PERKINS, R.J. 1998 Shape oscillations of rising bubbles. *Appl. Sci. Res.* **58**, 387–408.

MAGNAUDET, J., TAKAGI, S. & LEGENDRE, D. 2003 Drag, deformation and lateral migration of a buoyant drop moving near a wall. *J. Fluid Mech.* **476**, 115–157.

MANICA, R., KLASEBOER, E. & CHAN, D.Y.C. 2016*a* The hydrodynamics of bubble rise and impact with solid surfaces. *Adv. Colloid Interface Sci.* **235**, 214–232.

MANICA, R., KLASEBOERA, E. & CHAN, D.Y.C. 2016*b* The impact and bounce of air bubbles at a flat fluid interface. *Soft Matt.* **12**, 3271.

MARZO, A., SEAH, S.A., DRINKWATER, B.W., SAHOO, D.R., LONG, B. & SUBRAMANIAN, S. 2015 Holographic acoustic elements for manipulation of levitated objects. *Nat. Commun.* **6**, 8661.

MATHAI, V., ZHU, X., SUN, C. & LOHSE, D. 2017 Mass and moment of inertia govern the transition in the dynamics and wakes of freely rising and falling cylinders. *Phys. Rev. Lett.* **119**, 054501.

MEJIA-ALVAREZ, R., OHTAKE, T. & FOSS, J.A. 2021 A levitating/rotating ball–basic considerations. *Exp. Fluids* **62**, 243.

MENDELSON, H.D. 1967 The prediction of bubble terminal velocities from wave theory. *AIChE J.* **13**, 250–253.

MIRICA, K.A., SHEVKOPLYAS, S.S., PHILLIPS, S.T., GUPTA, M. & WHITESIDES, G.M. 2009 Measuring density of solids and liquids using magnetic levitation: fundamentals. *J. Am. Chem. Soc.* **131** (29), 10049–10058.

OCKENDON, H., OCKENDON, J.R. & MULLIN, T. 2024 Thin-film flow between a rotating sphere and a nearly vertical moving plate. *J. Fluid Mech.* **988**, A7.

OGUZ, H.N. & PROSPERETTI, A. 1998 The natural frequency of oscillation of gas bubbles in tubes. *J. Acoust. Soc. Am.* **103**, 3301–3308.

ORTIZ-VILLAFUERTE, J., SCHMIDL, W.D. & HASSAN, Y.A. 2001 Rocking motion, trajectory and shape of bubbles rising in small diameter pipes. *Expl Therm. Fluid Sci.* **25**, 43–53.

SEGRE, G. & SILBERBERG, A. 1962 Behaviour of macroscopic rigid spheres in Poiseuille flow part 1. Determination of local concentration by statistical analysis of particle passages through crossed light beams. *J. Fluid Mech.* **14** (1), 115–135.

SHE, W.-X., GAO, Q., ZUO, Z.-Y., LIAO, X.-W., ZHAO, L., ZHANG, L.-X., NIE, D.-M. & SHAO, X.-M. 2021 Experimental study on a zigzagging bubble using tomographic particle image velocimetry with shadow image reconstruction. *Phys. Fluids* **33**, 083313.

STAN, C.A., ELLERBEE, A.K., GUGLIELMINI, L., STONE, H.A. & WHITESIDES, G.M. 2013 The magnitude of lift forces acting on drops and bubbles in liquids flowing inside microchannels. *Lab on a Chip* **13**, 365.

TAKEMURA, F., TAKAGI, S., MAGNAUDET, J. & MATSUMOTO, Y. 2002 Drag and lift forces on a bubble rising near a vertical wall in a viscous liquid. *J. Fluid Mech.* **461**, 277–300.

TRINH, E.H. 1985 Compact acoustic levitation device for studies in fluid dynamics and material science in the laboratory and microgravity. *Rev. Sci. Instrum.* **56** (11), 2059.

https://doi.org/10.1017/jfm.2025.10837 Published online by Cambridge University Press